12th IFAC International Symposium on
Advanced Control of Chemical Processes
July 14-17, 2024. Toronto, Canada

Thermodynamic model identification for a one-stage spray dryer

A. Lepsien [*,**], **A. Schaum** [*,**]

[*] *Department of Process Analytics, University of Hohenheim, Stuttgart, Germany*
e-mail: {arthur.lepsien;alexander.schaum}@uni-hohenheim.de
[**] *Computational Science Hub, University of Hohenheim, Stuttgart, Germany*

Abstract: The present work deals with the identification of a thermodynamic model for a one–stage spray drying tower. Motivated by the underlying time-scale separation for thermodynamic (slow) and dried powder specific (fast) states, in this first step the focus lies on the description of all relevant thermodynamic mechanisms which determine the resulting Particle Size Distribution (PSD) of the dried powder. Different to models discussed in the literature for similar drying processes, the model explicitly takes into account changes in the flow rates and densities due to evaporation, and proposes a simple monotonic dependency of the evaporation rate motivated by Monod kinetics from bioprocess modeling. The model parameters are partially taken from the literature and partially identified using a least squares procedure on the basis of experimental data. The experiments performed are parameter combinations of the spray tower configuration, which result in different particle size distributions and provide important information about the potential for future steps toward process monitoring and feedforward–feedback control to achieve desired PSDs.

Keywords: Spray drying, thermodynamics, model identification, parameter estimation

1. INTRODUCTION

Spray drying is an important process in the manufacturing of powdered products, in which a liquid is converted into fine particles by being sprayed through a nozzle and then dried by hot air during the transition through the drying chamber. The particle size distribution is a crucial factor that determines the quality and (bio-)compatibility of the resulting powder with, e.g. the human respiratory system or factory conveyor systems. The cost-effectiveness of the overall process is greatly influenced by the conditions and reproducibility of the process. Improving process stability with regard to changing disturbances, i.e. different lab or manufacturing conditions and product quality, requires modeling and parameter identification to obtain reliable simulation models that can be used for process design, monitoring and control.

The two main different categories of spray dryer models are the ones to monitor the system behavior of an existing dryer in time, i.e. dynamic simulations, and those for designing an optimal dryer to fulfill certain conditions, i.e. design simulations. These two modeling approaches differ generally, as they are intended for different goals and inhibit different kinds of model approximations.

Some of the advanced models currently in use are capable of simulating complex phenomena, including heat and mass transfer, evaporation, droplet breakup, particle aggregation, and more. Most of the complex models have a high computational effort and are thus not real-time applicable. These include detailed Computational Fluid Dynamics (CFD) models for static design oriented simulation (Woo et al., 2008; Gopireddy and Gutheil, 2013). Common models for dynamic simulation, as models for (thermo)dynamic simulation with real-time capability, are linear models designed for control design that are also used for closed-loop simulation such as in (Clarke, 1988; Tan et al., 2009, 2011), and lumped, nonlinear first-principles engineering models as in (Govaerts et al., 1994; Langrish, 2009; Petersen, 2016; Sarkar, 2003). The purpose of the dynamic simulation models is often to enable control and estimation schemes for the process at hand. In the literature there is a lack of observers to estimate the nonlinear drying thermodynamics. A single-stage dynamic model is developed by (Govaerts et al., 1994) for the simulation of the residual moisture control and air temperatures in an industrial spray drying process. There, changes in the amount of vapor are ignored in the mass balance equations, which will be done different here. The moisture content for drying of milk powders in a spouted bed dryer is described by a physical-mathematical model in (Vieira et al., 2015). Here, evaporation of the liquid phase is estimated using a neural network.

A detailed review of the status and future of modeling and control for spray drying of dairy products is given in (O'Callaghan and Cunningham, 2005) and in (Akter et al., 2022) for food.

With the modeling of the spray drying process, there exist different scales for the modeling, c.f. (Langrish, 2009). These scales represent the types of physical phenomena and the magnitude of interactions described by the under-

lying model. The largest scale deals with the modeling of thermodynamics based on first principle mass and energy balances. The medium scale is concerned with parallel spray towers, in which both spray gas and solution are sprayed down in parallel at the inlet at the top. The resulting trajectories are then estimated utilizing momentum conservation and the drying of the particles is introduced via a reduction in the surface area as a coupling. The finest scale solves partial continuity, momentum, and energy dissipation equations, which leads to methods of CFD. With finer scaling of the model, the computational complexity rises. In every spray drying process, there are, additionally to the different size scales, two different time scales at play.

The preceding studies have provided a solid basis for the modelling of spray dryers for the purpose of process monitoring and control, but have left some central questions unanswered. In particular, in contrast to (Petersen et al., 2013, 2015; Petersen, 2016) in this work, the outflow rate of the gas phase is fixed by an aspirator (see Fig. 2 below). Therefore, the difference between gas phase inflow and outflow due to water evaporation needs to be taken into account explicitly. Along with this goes a difference between liquid densities at in- and outlet, which were also not accounted for in (Petersen, 2016). Furthermore, the reported evaporation rates required adaptation to fit to the experimental data.

2. PROBLEM DESCRIPTION

In this work, a nonlinear model for a one–stage spray dryer is derived with first-principles. The parameters of the model are estimated with step responses of the spray–dryer. The resulting model is real-time capable and used for observation of the immeasurable powder moisture content inside the drying chamber. In the spray dryer, the two different time scales describe the slow thermodynamics and the fast particle dynamics due to the small residence time inside the drying chamber. These two time scales can be modeled with Singular Pertubation Theory (SPT) as

$$\dot{\boldsymbol{x}} = \boldsymbol{f}(\boldsymbol{x}, \boldsymbol{u}, p), \tag{1a}$$
$$\boldsymbol{y} = \boldsymbol{h}(\boldsymbol{x}, \boldsymbol{u}), \tag{1b}$$
$$\epsilon \dot{p} = \mathcal{L}\left[\boldsymbol{x}, \boldsymbol{u}\right]\{p\}, \tag{1c}$$
$$y_p = \bar{p}(\boldsymbol{x}, \boldsymbol{u}, s, t), \tag{1d}$$

where $\epsilon \ll 1$ represents the time scale variation and $\boldsymbol{x} \in \mathbb{R}^n, \boldsymbol{u} \in \mathbb{R}^p, \boldsymbol{y} \in \mathbb{R}^m$ represent the thermodynamic state, input and output variables, respectively. The functions $\boldsymbol{f} : \mathbb{R}^n_+ \times \mathcal{H} \times \mathbb{R}^p \to \mathbb{R}^n$ and $\boldsymbol{h} : \mathbb{R}^n_+ \to \mathbb{R}^m$ represent the thermodynamic dynamics with respect to both time scales. The operator $\mathcal{L}[\boldsymbol{x}, \boldsymbol{u}] : \mathcal{H} \to \mathcal{H}$ maps suitable function spaces $\mathcal{H}$ and is dependent on the thermodynamic system state. It describes the PSD Probability Density Function (PDF) $p(\boldsymbol{x}, \boldsymbol{u}, s, t)$ evolution with respect to time t and particle size s. Possible operators can be found within Fokker-Planck Equation (FPE) or Population Balance Equation (PBE) schemes. It should be noted, that in many applications the particle size outlet measurements are only available occasionally. In this approach, the main control interest lies on the slow manifold of the thermodynamics which couple back onto the particle size distribution properties. A discontinuous change in spray rate $\dot{v}_{\mathrm{p,in}}$ during process runtime, leads to a change in the final PSD PDF $\bar{p}_f$ of the spray drying process.

To account for these thermodynamic dependencies, a first–principle lumped model of the spray dryer needs to be derived and a parameter identification problem solved. The resulting system should be real–time capable, to predict the thermodynamic changes of the drying unit and the resulting PSD in real–time. According to (1) the slow thermodynamic states determine the time evolution on the fast time scale of the particle dynamics and thus represent the dominant variables which need to be controlled to achieve a desired PSD for the sprayed powder. These thermodynamic state variables in turn can not be controlled directly but only through appropriately choosing the inlet concentration, liquid volume flow, air flow and air inlet temperature. Thus, a model for providing good predictions for the PSD requires first a precise modeling of the thermodynamic state variables and their functional dependencies on the described input variables. This motivates the present study as a first inductive step towards (i) a more complete description of this complex interplay and (ii) monitoring and control design approaches exploring the underlying structural properties.

Fig. 1 shows the difference between two PSD measurements with fixed process conditions at different times of the year, leading to differences in external system disturbances. A shift in the mode is clearly recognizable and can be assigned to the external thermodynamic influencing factors. For this reason, it is important to model the thermodynamic effects in the spray tower sufficiently well so that an accurate prediction of the experimental final PSD $\bar{p}_f$ in (1) is possible.

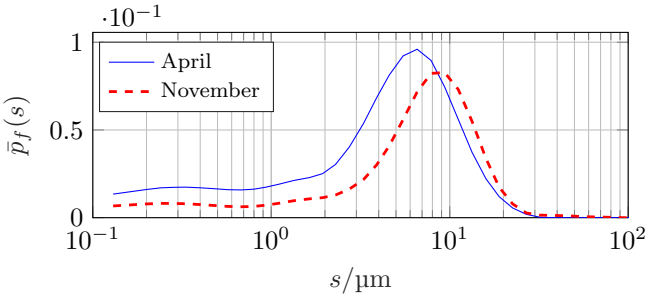

Fig. 1. Comparison between April and November PSD measurements with $\dot{v}_{\mathrm{p,in}} = 1.81\,\mathrm{mL\,min^{-1}}$ to visualize influence of external parameters on the final PSD $\bar{p}_f$.

3. THERMODYNAMIC MODEL

In the following, the thermodynamic model for a general one–stage spray dryer is derived. A steady-state particle size control for each discretization step can be designed using thermodynamic coupling. This allows the prediction of future PSDs and thus the possibility of feedforward feedback designs for PSD control.

The schematic representation of the dryer is visible in Figure 2. For this paper, the thermodynamic model of the spray dryer should fulfill certain conditions, similar to (Petersen et al., 2013, 2015; Petersen, 2016). Firstly, the model needs to be on a time scale on which the measurements are taken, i.e. internal diffusion processes inside the droplets can be ignored. Secondly, the turbulent flow inside the spray dryer shall be ignored, as well.

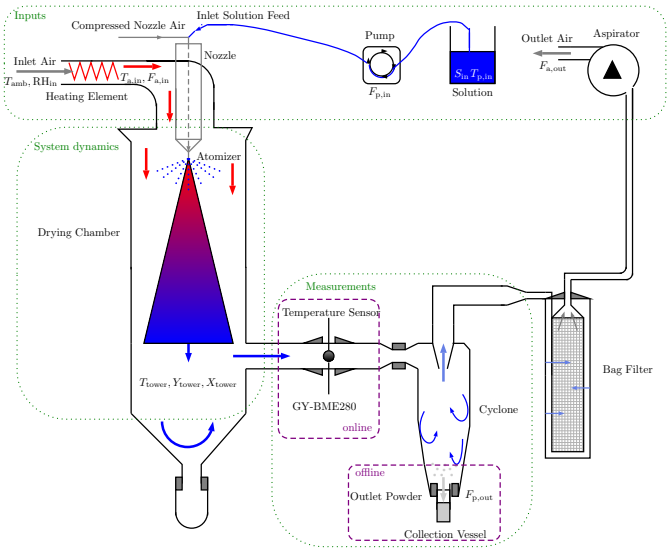

Fig. 2. Principle arrangement of the Mini Büchi B290.

This leads to a model without consideration of the linear momentum equations inside the spray dryer. Finally, the thermodynamic equations have to be identifiable for the given spray dryer and measurement possibilities, e.g. the particle size at the outlet and the moisture content in the powder are typically not real-time measurable. Additionally, the model should consist of concentrated elements, i.e. be a lumped model. The model uncertainties and simplifications can be corrected with a suitable observer later on, and the dependence of the thermodynamic states on the PSD p can be identified in a second step.

The above considerations lead to a coupled system of nonlinear Ordinary Differential Equations (ODEs) for the thermodynamics, governed by mass and energy balance equations. These model equations can be derived with the following simplification assumptions:

(A.1) Air and water vapor are assumed as ideal gases.

(A.2) The air and the powder inside the tower are in thermal equilibrium, i.e. $T^{\mathrm{a}}_{\mathrm{tower}} = T^{\mathrm{p}}_{\mathrm{tower}}$.

(A.3) The tower is under constant atmospheric pressure, i.e. $P_{\mathrm{tower}} = P_0 = \text{const.}$.

(A.4) No accumulation of powder or air occurs inside the tower, i.e. $\dot{m}_{\mathrm{p,in}} + \dot{m}_{\mathrm{a,in}} = \dot{m}_{\mathrm{p,out}} + \dot{m}_{\mathrm{a,out}}$ This implies constant masses of solid material m_{s} and dry air m_{da}, respectively.

(A.5) Due to the aspirator, the volume flow of air out of the tower $\dot{v}_{\mathrm{a,out}} = \dot{v}_{\mathrm{aspirator}}$ is set, the air volume sucked into the tower thus results in the difference of the aspirator volume flow with the water evaporation R_{w}

$$\dot{v}_{\mathrm{a,in}} = \dot{v}_{\mathrm{aspirator}} - \frac{R_{\mathrm{w}}}{\rho_{\mathrm{v}}}. \tag{2}$$

With Assumption (A.1), the water vapor density ρ_{v} follows from the ideal gas law. It reads

$$\rho_{\mathrm{v}} = \frac{M_{\mathrm{v}} P_0}{R T_{\mathrm{tower}}}. \tag{3}$$

Following this logic, the volume flow of liquid into the tower $\dot{v}_{\mathrm{p,in}} = \dot{v}_{\mathrm{pump}}$ is fixed, the liquid-solid mixture getting deposited in the collection vessel results by $\dot{m}_{\mathrm{s,in}} = \dot{m}_{\mathrm{s,out}}$ to

$$\dot{v}_{\mathrm{p,out}} = \dot{v}_{\mathrm{p,in}} \frac{S_{\mathrm{in}}}{S_{\mathrm{tower}}}, \tag{4}$$

with inlet concentration S_{in} and tower concentration S_{tower}, as defined in (7) below. This is a different assumption to the model derived in (Petersen, 2016), as there the volume flow deviation with water evaporation is not taken into account.

(A.6) The tower and the powder are assumed to be well mixed (lumped model), s.t. there is no concentration gradient in the inlet liquid feed and there is no temperature, humidity or moisture gradient along the tower extension.

(A.7) For the energy balance kinetic and potential energies of the powder can be neglected, i.e. $E^{\mathrm{p,a}}_{\mathrm{kin}}, E^{\mathrm{p,a}}_{\mathrm{pot}} \ll U_{\mathrm{tower}}$. This leads to

$$\dot{U} = \Delta H + Q, \tag{5}$$

with the change in enhalpy ΔH and heat Q.

With these assumptions, the spray dryer, sketched in Fig. 2, can be modeled as an open thermodynamic system, where powder mass is entering the system with the spray nozzle, the air is transported by the aspirator through the tower, and heating of the air takes place at the top of the drying chamber. The system can be identified with two in- and outlets for air and powder, respectively. All parameters used in the following, which were determined either by physical constants or empirical investigations, are shown in Table 1. For the mass balances, the mass fractions X and Y are defined as

$$X = \frac{m_{\mathrm{w}}}{m_{\mathrm{s}}}, \qquad Y = \frac{m_{\mathrm{v}}}{m_{\mathrm{da}}}, \tag{6}$$

with the total water mass m_{w}, solid mass m_{s}, vapor mass m_{v} and dry air mass m_{da}. The water content mass fraction of the powder X describes the amount of water per amount of solid in a given particle. Similarly, the water content mass fraction of the air Y describes the amount of vaporized water per amount of dry air. The mass concentration $S \in [0, 1]$ is defined as

$$S = \frac{m_{\mathrm{s}}}{m_{\mathrm{s}} + m_{\mathrm{w}}} = \frac{m_{\mathrm{s}}}{m_{\mathrm{p}}}, \tag{7}$$

and describes the amount of solid per total mass of the droplet/particle. As the solid content cannot evaporate, $m_{\mathrm{s}} = \text{const.}$, but m_{w} is a function of time.. From the above equations the relation between S and X results to

$$S = \frac{1}{1+X}, \qquad X = \frac{1-S}{S}. \tag{8}$$

The (powder) feed mass flow $[F] = \mathrm{kg\,s^{-1}}$ is regulated by the pump volumetric flow $[\dot{v}] = \mathrm{mL\,s^{-1}}$ and is composed of

$$F_{\mathrm{p,in}} = \dot{v}_{\mathrm{p,in}} \left(\rho_{\mathrm{s}} S_{\mathrm{in}} + \rho_{\mathrm{w}} \left[1 - S_{\mathrm{in}}\right]\right), \tag{9}$$

$$F_{\mathrm{p,out}} = \dot{v}_{\mathrm{p,out}} \left(\rho_{\mathrm{s}} S_{\mathrm{tower}} + \rho_{\mathrm{w}} \left[1 - S_{\mathrm{tower}}\right]\right), \tag{10}$$

with the densities of the solid ρ_{s} and water ρ_{w}. The air feed mass flow F_{a} is regulated by the aspirator volume flow $\dot{v}_{\mathrm{a,out}}$. With the assumptions of constant dryer pressure P_0 (A.3) and ideal gas (A.1), the density ρ results in

$$M \frac{P_0 V}{RT} = nM \Rightarrow \frac{M P_0}{RT} = \frac{nM}{V} = \rho, \tag{11}$$

with the molar mass M, amount of material n, volume V, temperature T and universal gas constant R leading to

$$F_{\mathrm{a,in}} = \dot{v}_{\mathrm{a,in}}\rho_{\mathrm{a,in}} = \dot{v}_{\mathrm{a,in}}\frac{M_{\mathrm{a,in}}P_0}{RT_{\mathrm{a,in}}}, \tag{12}$$

$$F_{\mathrm{a,out}} = \dot{v}_{\mathrm{a,out}}\rho_{\mathrm{a,out}} = \dot{v}_{\mathrm{a,out}}\frac{M_{\mathrm{a,out}}P_0}{RT_{\mathrm{tower}}}. \tag{13}$$

Note, that in (12) the heated air inlet temperature is used, as the density of the air is with respect to the heated air.

The molar mass of air M_{a} consists of water vapor and dry air, where the molar mass for water and water vapor satisfies $M_{\mathrm{w}} = M_{\mathrm{v}}$ as the water being mixed to the powder is demineralized or distilled. Dry air consists of different molecules and can be modeled as a uniformly distributed average of these components, following the approach in (Lide, 2004). These two form together the molar mass of the air entering and leaving the system with their respective mass balance as

$$M_{\mathrm{a}} = \frac{Y}{1+Y}M_{\mathrm{w}} + \frac{1}{1+Y}M_{\mathrm{da}} \tag{14}$$

The balancing of the molar masses is also different from (Petersen, 2016), as in the literature the water densities and thus the molar masses at in- and outlet are assumed to be the same. From this, the dry air inlet flow can be calculated with the approach in (Petersen et al., 2013). To account for the difference in air and dry air entering and exiting the system, the mass fraction of dry air m_{da} to total air mass m_{a} needs to be accounted for. The dry air flow thus reads

$$F_{\mathrm{da}} = \frac{1}{1+Y}F_{\mathrm{a}}, \tag{15}$$

The inlet water vapor fraction results from a negative partial pressure deviation from the saturation pressure, c.f. (Petersen, 2016), according to the relative humidity at the inlet $\mathrm{RH}_{\mathrm{in}}$. Generally, the relative humidity can be calculated with the ratio of partial pressure P_{v} to saturation pressure $P_{\mathrm{v}}^{\mathrm{sat}}$, i.e.,

$$\overline{\mathrm{RH}} = \frac{P_{\mathrm{v}}}{P_{\mathrm{v}}^{\mathrm{sat}}}. \tag{16}$$

Here, the relative humidity is considered as a numeric value, and thus the factor of 100 is dropped and this is indicated by $(\bar{\cdot})$. From this, and following the approach in (Petersen et al., 2013, 2015), the inlet water vapor fraction can be calculated to be

$$Y_{\mathrm{in}} = \frac{M_{\mathrm{v}}}{M_{\mathrm{da}}}\frac{\overline{\mathrm{RH}}_{\mathrm{in}}P_{\mathrm{v}}^{\mathrm{in,sat}}(T_{\mathrm{amb}})}{P_0 - \overline{\mathrm{RH}}_{\mathrm{in}}P_{\mathrm{v}}^{\mathrm{in,sat}}(T_{\mathrm{amb}})}. \tag{17}$$

It is important to note that this formula specifically describes the fraction of the incoming air before it reaches the heating element in the spray dryer, as Y_{in} should describe the air mass fraction entering the tower unit at the air inlet. The saturation pressure $[P_{\mathrm{v}}^{\mathrm{sat}}] = \mathrm{Pa}$ can be calculated with the Antoine equation described in (Smith et al., 2018; Thomson, 1946) as

$$P_{\mathrm{v}}^{\mathrm{sat}}(T) = \exp\left[A - \frac{B}{T + C - 273.15\,^{\circ}\mathrm{C}}\right]\cdot 1000\ \mathrm{Pa}, \tag{18}$$

which is valid for T within the range of 0 °C to 200 °C. As the values of B and C are given for temperatures in °C but T is in K, the constant $-273.15\,^{\circ}\mathrm{C}$ is added to the denominator. For the model, first the mass balance equation for the water content mass fraction in the powder X_{tower} shall be derived. A Monod-like approach as in (Monod, 1949; Srinivasan, 2022) is used for the water evaporation rate with hyperbolic character

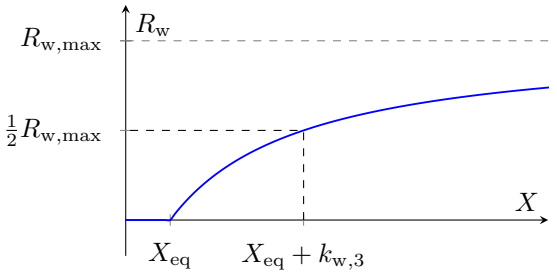

Fig. 3. Visualization of the Monod kinetic part of the water evaporation rate R_{w}.

$$R_{\mathrm{w}} = k_{\mathrm{w,1}}\exp\left[-\frac{k_{\mathrm{w,2}}}{R}\left(\frac{1}{T}-\frac{1}{T_0}\right)\right]\frac{m_{\mathrm{s}}\left[X - X_{\mathrm{eq}}(T,Y)\right]}{k_{\mathrm{w,3}} + (X - X_{\mathrm{eq}}(T,Y))}. \tag{19}$$

The visualization of the evaporation rate in function of X can be seen in Fig. 3. Here, $R_{\mathrm{w,max}} = k_{\mathrm{w,1}}\exp[\cdot]m_{\mathrm{s}}$ is the maximum growth factor of the water evaporation and $k_{\mathrm{w,3}}$ is the half-saturation constant. For the given measurement data, this approach seems to be better suited than the proposed function in (Petersen et al., 2013, 2015), and thus will be used in the following.

The Equlibrium Moisture Content (EMC) X_{eq} can be modeled with the Guggenheim-Anderson-de Boer (GAB) equation (Basu et al., 2006; Nurhadi and Roos, 2016), describing adsorption and desorption isotherms. It states that, as relative humidity increases, the EMC increases proportionally, but it decreases with increasing temperature. The formula reads

$$X_{\mathrm{eq}}(T,Y) = \frac{X_{0,\mathrm{eq}}C_{\mathrm{eq}}K_{\mathrm{eq}}\overline{\mathrm{RH}}}{(1-K_{\mathrm{eq}}\overline{\mathrm{RH}})(1-K_{\mathrm{eq}}\overline{\mathrm{RH}}+C_{\mathrm{eq}}K_{\mathrm{eq}}\overline{\mathrm{RH}})} + X_{\mathrm{add}}. \tag{20}$$

The parameters $X_{0,\mathrm{eq}}$, K_{eq}, and C_{eq} follow the approach in (Calvert, 1990), and are thus expressed with Arrhenius like equations

$$\{X_0, K, C\}_{\mathrm{eq}} = \{X_0, K, C\}'\exp\left[\frac{-\Delta H_{\{X,K,C\}}}{RT}\right]. \tag{21}$$

The relation between absolute air humidity and relative humidity follows from (16)-(17) to be

$$\overline{\mathrm{RH}}(T,Y) = \frac{Y}{\frac{M_{\mathrm{v}}}{M_{\mathrm{da}}}+Y}\frac{P_0}{P_{\mathrm{v}}^{\mathrm{sat}}(T)}. \tag{22}$$

With the above equations the ODE for the water mass fraction inside the powder X_{tower} can be formulated. Considering constant solid mass content from Assumption (A.4), i.e. $m_{\mathrm{s}} = \mathrm{const.}$, it follows that

$$\dot{X}_{\mathrm{tower}} = \frac{\dot{m}_{\mathrm{w}}}{m_{\mathrm{s}}} = \frac{1}{m_{\mathrm{s}}}\Big(F_{\mathrm{p,in}}X_{\mathrm{in}} - F_{\mathrm{p,out}}X_{\mathrm{tower}} - R_{\mathrm{w}}\Big). \tag{23}$$

The next step is to derive the ODE for the moisture content mass fraction of water vapor in the air Y_{tower}. Note, that in the literature Y is sometimes also called absolute humidity. The ODE is based on a net flow balance of the supply and exhaust air. Accounting for a constant dry air mass from Assumption (A.4), i.e. $m_{\mathrm{da}} = \mathrm{const.}$, one has

$$\dot{Y}_{\mathrm{tower}} = \frac{\dot{m}_{\mathrm{v}}}{m_{\mathrm{da}}} = \frac{1}{m_{\mathrm{da}}}\Big(F_{\mathrm{a,in}}Y_{\mathrm{in}} - F_{\mathrm{a,out}}Y_{\mathrm{tower}} + R_{\mathrm{w}}\Big). \tag{24}$$

The last state equation shall describe the energy balance in the system. With neglectable kinetic and potential energy and vanishing flow work of Assumption (A.7), one has four

specific enthalpies in the system: two at the inlet, $h_{\mathrm{a,in}}$, $h_{\mathrm{p,in}}$ and two at the outlet $h_{\mathrm{a,out}}$, $h_{\mathrm{p,out}}$. These are under the influence of the temperature of the heated inlet air $T_{\mathrm{a,in}}$, solution inlet temperature $T_{\mathrm{p,in}}$, and tower air T_{tower}. The enthalpies can be formulated with the approach in (Petersen et al., 2013; Smith et al., 2018) on the basis of weighted heat capacities under consideration of $m_{\mathrm{p}} = m_{\mathrm{s}} + m_{\mathrm{w}}$ to be

$$h_{\mathrm{a}} = \left(c_{\mathrm{da}}(T_{\mathrm{a}}) \frac{1}{1+Y} + c_{\mathrm{v}}(T_{\mathrm{a}}) \frac{Y}{1+Y} \right) T_{\mathrm{a}}, \tag{25}$$

$$h_{\mathrm{p}} = \left(c_{\mathrm{s}}(T_{\mathrm{p}}) S + c_{\mathrm{w}}(T_{\mathrm{p}})(1-S) \right) T_{\mathrm{p}}, \tag{26}$$

with temperature-dependent heat capacities of dry air c_{da}, water vapor c_{v}, liquid water c_{w} from (Smith et al., 2018) and solid (mannitol) c_{s} from (Tong et al., 2010). The mass fraction for the solid has to be divided by the molar mass of the solid, as the parameterized formula in (Tong et al., 2010) gives the result in $[\mathrm{J\,K^{-1}\,mol^{-1}}]$ but $[\mathrm{J\,K^{-1}\,kg^{-1}}]$ is needed. Additionally, the heat loss can be modeled according to

$$Q_{\mathrm{loss}} = k \left(T_{\mathrm{tower}} - T_{\mathrm{amb}} \right), \tag{27}$$

with thermal conductivity k. The heat of evaporation consists of

$$Q_{\mathrm{evap}} = \lambda(T_{\mathrm{tower}}) R_{\mathrm{w}} = \lambda_{\mathrm{ref}} \left(\frac{1 - \frac{T_{\mathrm{tower}}}{\alpha}}{1 - \frac{T_{\mathrm{ref,evap}}}{\alpha}} \right)^{\beta} R_{\mathrm{w}}, \tag{28}$$

with $\alpha, \beta, \lambda_{\mathrm{ref}}, T_{\mathrm{ref,evap}}$ as in (Smith et al., 2018) see also Table 1). From these considerations, the ODE for thermal energy can be formulated with the above and (5) to

$$\begin{aligned} \dot{T}_{\mathrm{tower}} = \frac{1}{C_{\mathrm{thermal}}} \Big[& F_{\mathrm{a,in}} h_{\mathrm{a,in}} - F_{\mathrm{a,out}} h_{\mathrm{a,out}} + \dots \\ & F_{\mathrm{p,in}} h_{\mathrm{p,in}} - F_{\mathrm{p,out}} h_{\mathrm{p,out}} - Q_{\mathrm{evap}} - Q_{\mathrm{loss}} \Big], \end{aligned} \tag{29}$$

with $[C_{\mathrm{thermal}}] = \mathrm{J\,K^{-1}}$.

3.1 Modifications

The above equations can be adapted such, that they account for unmodeled physical phenomena, such as air leakages, the turbulent flow and temperature distribution inside the tower, uneven temperature distribution inside the particles (diffusive process). Furthermore the violations of the assumptions to set up the simplified model equations should be accounted for with empirical parameters (Petersen et al., 2015). The constants $Y_{\mathrm{add}}, T_{\mathrm{add}}$ and F_{add} are added to the system equations. These have to be fitted for each given spray dryer separately. The modified equations read (23) and

$$\begin{aligned} \dot{Y}_{\mathrm{tower}} = \frac{1}{m_{\mathrm{da}}} \Big[& F_{\mathrm{a,in}} Y_{\mathrm{in}} - F_{\mathrm{a,out}} Y_{\mathrm{tower}} + \dots \\ & R_{\mathrm{w}} + F_{\mathrm{add}} Y_{\mathrm{add}} - F_{\mathrm{add}} Y_{\mathrm{tower}} \Big] \end{aligned} \tag{30}$$

$$\begin{aligned} \dot{T}_{\mathrm{tower}} = \frac{1}{C_{\mathrm{thermal}}} \Big[& F_{\mathrm{a,in}} h_{\mathrm{a,in}} - F_{\mathrm{a,out}} h_{\mathrm{a,out}} + \\ & F_{\mathrm{p,in}} h_{\mathrm{p,in}} - F_{\mathrm{p,out}} h_{\mathrm{p,out}} - Q_{\mathrm{evap}} - Q_{\mathrm{loss}} \\ & - F_{\mathrm{add}} h_{\mathrm{a,out}} + F_{\mathrm{add}} h_{\mathrm{a,add}}(T_{\mathrm{tower}}) \Big], \end{aligned} \tag{31}$$

Here $h_{\mathrm{a,add}}$ depends on the temperature, and the heat capacities are temperature–dependent.

4. PARAMETER IDENTIFICATION

For the spray drying experiments crystalline Mannitol was used (Pearlitol 160 C, Roquette, France; batch E992Y) and prepared in an aqueous, well–stirred solution. The spray drying experiments were carried out with the lab–scale tabletop spray–dryer Mini Büchi B-290 (Büchi, Flawil, Switzerland) equipped with a high performance cyclone and a two fluid nozzle with 0.7 mm of inner and 1.4 mm of outer diameter (all Büchi). For the dispersing air in the nozzle pressured air was used and set with a rotameter to 50 mm equivalent to $601\,\mathrm{L\,h^{-1}}$. An aspirator output 100 % power was chosen, which correlates to an airflow of $35\,\mathrm{m^3\,h^{-1}}$ through the spray dryer. The spray dryer has a serial port to monitor some physical parameters of the spray-drying tower. It can be used to track the inlet and outlet temperatures and the flow rate of the feed. To measure the humidity contents at the inlet and outlet of the tower in addition to the ambient temperature, two GY-BME 280 sensors in connection with an Arduino Uno are used. Calibration of the sensors is done with a testo 435-4 - Multi-function indoor air quality meter.

With the above equations a state space system description can be formulated with the input vector

$$\boldsymbol{u} = \left[\dot{v}_{\mathrm{pump}} \;\; \dot{v}_{\mathrm{aspirator}} \;\; S_{\mathrm{in}} \;\; T_{\mathrm{a,in}} \right]^{\mathrm{T}}, \tag{32}$$

and state vector

$$\boldsymbol{x} = \left[X_{\mathrm{tower}} \;\; Y_{\mathrm{tower}} \;\; T_{\mathrm{tower}} \right]^{\mathrm{T}}. \tag{33}$$

As the system undergoes non-controllable disturbances in form of ambient properties of the room, i.e. exogenous inputs, these can be modeled as a disturbance

$$\boldsymbol{d} = \left[T_{\mathrm{p,in}} \;\; T_{\mathrm{amb}} \;\; \overline{\mathrm{RH}}_{\mathrm{in}} \;\; P_{\mathrm{in}} \right]^{\mathrm{T}}. \tag{34}$$

The inlet relative humidity acts as a disturbance, as it is not directly controllable. It can only be influenced by connecting and switching on the dehumidifier before the air is entering the inlet of the tower. The measurable thermodynamic quantities are the temperature at the outlet T_{tower} and the relative humidity in the tower $\mathrm{RH}_{\mathrm{tower}}$. From these the output vector function can be derived, as T_{tower} is a state in itself and the relative humidity can be calculated from the moisture content Y_{tower} and the saturation pressure $P_{\mathrm{v}}^{\mathrm{sat}}$ by Antoine's Equation (cp. (18)). Thus the output function reads

$$\boldsymbol{y} = \boldsymbol{h}_{\mathrm{thermo}}(\boldsymbol{x}, \boldsymbol{u}, \boldsymbol{d}) = \begin{bmatrix} T_{\mathrm{tower}} \\ \overline{\mathrm{RH}}_{\mathrm{tower}}(T_{\mathrm{tower}}, Y_{\mathrm{tower}}) \end{bmatrix}. \tag{35}$$

Summarizing, the state space representation of the thermodynamic system reads

$$\begin{aligned} \dot{\boldsymbol{x}} &= \boldsymbol{f}_{\mathrm{thermo}}(\boldsymbol{x}, \boldsymbol{u}, \boldsymbol{d}), \quad \forall t > 0, \boldsymbol{x}(0) = \boldsymbol{x}_0, \\ \boldsymbol{y} &= \boldsymbol{h}_{\mathrm{thermo}}(\boldsymbol{x}, \boldsymbol{u}, \boldsymbol{d}), \quad \forall t \geq 0. \end{aligned} \tag{36}$$

The parameters, to be identified for this model, are summarized in the parameter vector

$$\boldsymbol{p}_{\mathrm{thermo}} = \Big[m_{\mathrm{s}}, m_{\mathrm{da}}, C_{\mathrm{thermal}}, k_{\mathrm{w},1}, k_{\mathrm{w},2}, k_{\mathrm{w},3}, k, Y_{\mathrm{add}}, T_{\mathrm{add}}, F_{\mathrm{add}} \Big]. \tag{37}$$

It should be emphasized here, that the parameters of the heat capacities, the Antoine equation and others not listed here, are assumed to be known, e.g. from the literature. Their values and corresponding sources are summarized in Tab. 1. For the parameter identification problem of the thermodynamic parameter vector (37), step responses

in the spraying rate at constant inlet temperatures were recorded. The GAB equation parameters are fitted with a least-squares optimization based on adsorption isotherms given by Dynamic Vapor Sorption (DVS) measurements at different temperatures. It is based on measuring the water intake of an active ingredient under controlled conditions. In this case, a known amount of mannitol is placed in a compartment and then exposed to a stream of water vapor. The moisture in the water vapor is gradually increased and the water pickup of the mannitol is measured continuously until equilibrium is reached. Measurements are made at different temperatures, in this case, 20 °C, 30 °C, and 40 °C. The data obtained is then used to establish the moisture adsorption isotherms of mannitol, which represent the relationship between the relative humidity and the water uptake of the substance to get the parameters used in (20).

To get an initial guess for the parameter vector, the water evaporation rate should be higher than the inlet volume flow to ensure drying of the particles. The optimization problem for the thermodynamics with the measurements of tower temperature and relative humidity reads

$$\begin{aligned} &\arg\min_{\boldsymbol{p}_{\text{thermo}}} && \frac{1}{N}\sum_{k=1}^{N}\|\boldsymbol{y}(t_k)-\boldsymbol{y}_{\text{ODE}}(t_k;\boldsymbol{p}_{\text{thermo}})\|^2 \\ &\text{subject to} && \boldsymbol{p}_{\text{thermo}} > \boldsymbol{0}, \end{aligned} \tag{38}$$

where N is the number of discrete measurement points. Before each experiment including the temperature and humidity sensors, these were calibrated using a testo 435 measurement device.

The validation experiment fit can be seen in purple in Fig. 4. This optimization result shows, that the time constants for the temperature and relative humidity fit quite well, but there is an initial overshoot of the temperature. It should be noted, that the internal dynamics, described with X, also displayed in Fig. 4, are just optimized concerning the stationary solution which was only offline measurable. The temporal evolution of the internal dynamics is within the range of the measured powder moisture contents according to individual experiments. If this state would be online measurable, a better fit with the ODE system could be ensured. Additionally, Fig. 4 includes the estimation via an Extended Kalman Filter (EKF) with the measurements and system dynamics according to (36), cp. Kulikov and Kulikova (2013). The orange dashed lines show either the GY-BME 280 sensor measurements or the offline moisture content measurement of the powder. The resulting identified parameter vector can be found in Tab. 1. It can be seen clearly, that the EKF improves prediction accuracy and lowers the initial overshoot.

To further improve the modeling accuracy, the lower scale models can be analyzed and incorporated into the model. This can be done by, e.g. setting up impulse equations for the particle trajectories or solving partial differential continuity, momentum, or energy dissipation equations with drying boundary conditions on the particles, i.e. shrinkage in surface area due to drying. It has to be recalled, that for the purpose at hand the system complexity has to be at a level at which it can be used in real-time simulations for the purpose of process monitoring and control, what is subject of a different study.

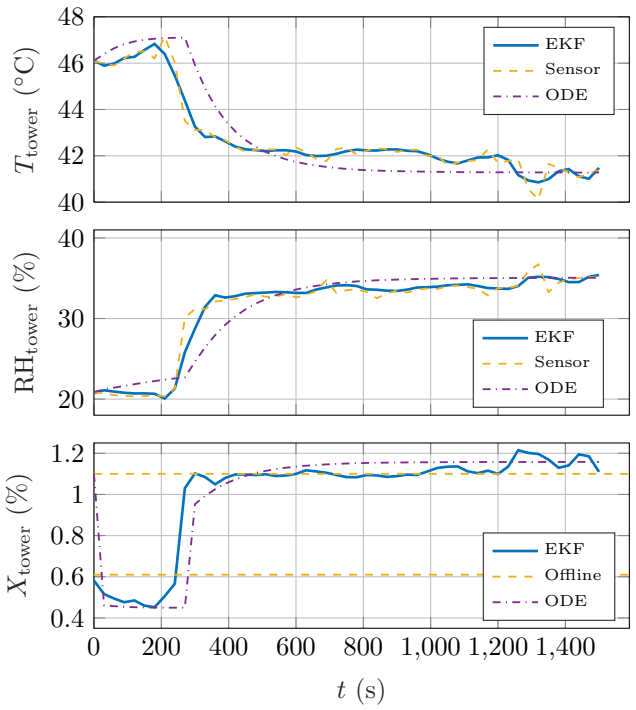

Fig. 4. Validation experiment results with a step in $\dot{v}_{\text{p,in}}$ from $1.81\,\text{mL}\,\text{min}^{-1}$ to $3.64\,\text{mL}\,\text{min}^{-1}$ after 240 s , EKF estimation in blue, parameters based on Table 1 lead to MSE of 0.7459, according to (38).

5. CONCLUSION

In this paper, a thermodynamic model for an one–stage spray drying tower is derived and identified. In comparison to previous studies concerned with similar setups some basic assumptions about the mass flows at inlet and outlet were adapted to explicitly account for changes due to water evaporation with impacts in flow rates, densities and the functional evaporation rate expression. The performance of the identified model is tested with experimental data. The model provides a basis for future studies that will concern the coupling with the dynamics of the PSD using process monitoring and feedforward-feedback control design approaches, making the real-time solvability of the resulting equations a central focus. Robustness, scalability and flexibility of the proposed system dynamics should be analysed in future works

REFERENCES

Akter, F., Muhury, R., Sultana, A., and Deb, U.K. (2022). A comprehensive review of mathematical modeling for drying processes of fruits and vegetables. International Journal of Food Science, 2022.

Basu, S., Shivhare, U.S., and Mujumdar, A.S. (2006). Models for sorption isotherms for foods: A review. Drying Technology, 24, 917–930. doi: 10.1080/07373930600775979.

Calvert, J.G. (1990). Glossary of atmospheric chemistry terms (recommendations 1990). Pure and Applied Chemistry, 62(11), 2167–2219.

Clarke, D.W. (1988). Application of generalized predictive control to industrial processes. IEEE Control systems magazine, 8(2), 49–55.

Gopireddy, S. and Gutheil, E. (2013). Numerical simulation of evaporation and drying of a bi-component droplet. International Journal of Heat and Mass Transfer, 66, 404–411.

Govaerts, R., Johnson, A., Crezee, R., Reyman, G., and Swinkels, P. (1994). Control of an industrial spray drying unit. Control Engineering Practice, 2(1), 69–85.

Kulikov, G.Y. and Kulikova, M.V. (2013). Accurate numerical implementation of the continuous-discrete extended kalman filter. IEEE Transactions on Automatic Control, 59(1), 273–279.

Langrish, T. (2009). Multi-scale mathematical modelling of spray dryers. Journal of Food Engineering, 93(2), 218–228.

Lide, D.R. (2004). CRC handbook of chemistry and physics, volume 85. CRC press.

Monod, J. (1949). The growth of bacterial cultures. Annual review of microbiology, 3(1), 371–394.

Nurhadi, B. and Roos, Y. (2016). Dynamic water sorption for the study of amorphous content of vacuum-dried honey powder. Powder Technology, 301, 981–988.

O'Callaghan, D. and Cunningham, P. (2005). Modern process control techniques in the production of dried milk products–a review. Le Lait, 85(4-5), 335–342.

Petersen, L.N. (2016). Economic Model Predictive Control for Spray Drying Plants. Ph.D. thesis, Technical University of Denmark.

Petersen, L.N., Jørgensen, J.B., and Rawlings, J.B. (2015). Economic optimization of spray dryer operation using nonlinear model predictive control with state estimation. IFAC-PapersOnLine, 48, 507–513.

Petersen, L.N., Poulsen, N.K., Niemann, H.H., Utzen, C., and Jørgensen, J.B. (2013). A grey-box model for spray drying plants. IFAC Proceedings Volumes (IFAC-PapersOnline), 10, 559–564.

Sarkar, I. (2003). MODELLING OF SPRAY DRYER. Ph.D. thesis, Indian Institute of Technology Roorkee.

Smith, J., Van Ness, H., and Abbott, M. (2018). Introduction to Chemical Engineering Thermodynamics. CHEMICAL ENGINEERING SERIES. McGraw-Hill Education.

Srinivasan, B. (2022). A guide to the Michaelis–Menten equation: steady state and beyond. The FEBS journal, 289(20), 6086–6098.

Tan, L.W., Ibrahim, M.N., Kamil, R., and Taip, F.S. (2011). Empirical modeling for spray drying process of sticky and non-sticky products. Procedia Food Science, 1, 690–697.

Tan, L., Taip, F., and Aziz, N.A. (2009). Simulation and control of spray drying using nozzle atomizer spray dryer. International Journal of Engineering and Technology, 9(10), 12–17.

Thomson, G.W. (1946). The antoine equation for vapor-pressure data. Chemical reviews, 38(1), 1–39.

Tong, B., Liu, R.B., Meng, C.G., Yu, F.Y., Ji, S.H., and Tan, Z.C. (2010). Heat capacities and nonisothermal thermal decomposition reaction kinetics of d-mannitol. Journal of Chemical & Engineering Data, 55(1), 119–124.

Vieira, G.N.A., Freire, F.B., and Freire, J.T. (2015). Control of the moisture content of milk powder produced in a spouted bed dryer using a grey-box inferential controller. Drying Technology, 33(15-16), 1920–1928.

Woo, M.W., Daud, W.R.W., Mujumdar, A.S., Wu, Z., Meor Talib, M.Z., and Tasirin, S.M. (2008). Cfd evaluation of droplet drying models in a spray dryer fitted with a rotary atomizer. Drying Technology, 26(10), 1180–1198.

Table 1. Model Parameters.

Context	Constant	Value	Unit
Fixed Parameters			
Density	ρ_{s}	1.514	$\mathrm{g\,mL^{-1}}$
	ρ_{w}	1.0	$\mathrm{g\,mL^{-1}}$
Molar Mass	M_{da}	28.9647	$\mathrm{g\,mol^{-1}}$
	M_{v}	18.01528	$\mathrm{g\,mol^{-1}}$
	M_{w}	18.01528	$\mathrm{g\,mol^{-1}}$
Gas Constant	R	8.3145	$\mathrm{J\,mol^{-1}\,K^{-1}}$
Antoine Equation	A	16.3872	–
	B	3885.7	°C
	C	230.17	°C
Thin-Layer Equation	T_0	298.15	K
Heat Capacities			
Dry Air	A_{da}	3.355	–
	B_{da}	$0.575 \cdot 10^{-3}$	$\mathrm{K^{-1}}$
	C_{da}	0	$\mathrm{K^{-2}}$
	D_{da}	$-0.016 \cdot 10^{5}$	$\mathrm{K^{2}}$
Water Vapor	A_{v}	3.470	–
	B_{v}	$1.450 \cdot 10^{-3}$	$\mathrm{K^{-1}}$
	C_{v}	0	$\mathrm{K^{-2}}$
	D_{v}	$0.121 \cdot 10^{5}$	$\mathrm{K^{2}}$
Liquid Water	A_{w}	8.712	–
	B_{w}	$1.25 \cdot 10^{-3}$	$\mathrm{K^{-1}}$
	C_{w}	$-0.18 \cdot 10^{-6}$	$\mathrm{K^{-2}}$
	D_{w}	0	$\mathrm{K^{2}}$
Solid Mannitol	$A_{\mathrm{s,m}}$	207.790	–
	$B_{\mathrm{s,m}}$	141.210	–
	$C_{\mathrm{s,m}}$	−23.623	–
	$D_{\mathrm{s,m}}$	−38.543	–
	$E_{\mathrm{s,m}}$	44.992	–
	$F_{\mathrm{s,m}}$	23.902	–
	$G_{\mathrm{s,m}}$	−32.126	–
	T_{min}	90	K
	T_{max}	390	K
Latent Heat of Evaporation	λ_{ref}	2257	$\mathrm{J\,g^{-1}}$
	$T_{\mathrm{ref,evap}}$	373.15	K
	α	647.1	K
	β	0.38	–
Identified Parameters			
Masses	m_{s}	0.0859	kg
	m_{da}	27.2720	kg
Thin-Layer Equation	$k_{\mathrm{w},1}$	0.0738	$\mathrm{s^{-1}}$
	$k_{\mathrm{w},2}$	$3.2576 \cdot 10^{4}$	$\mathrm{J\,mol^{-1}}$
	$k_{\mathrm{w},3}$	0.2370	–
GAB	X_0'	0.0377	$\mathrm{kg\,kg^{-1}}$
	K'	1.2350	$\mathrm{kg\,kg^{-1}}$
	C'	1.11540	$\mathrm{kg\,kg^{-1}}$
	ΔH_X	500	$\mathrm{J\,mol^{-1}}$
	ΔH_K	500	$\mathrm{J\,mol^{-1}}$
	ΔH_C	500	$\mathrm{J\,mol^{-1}}$
	X_{add}	0.0015	$\mathrm{kg\,kg^{-1}}$
Heat Loss	k_{UA}	0.0572	$\mathrm{W\,K^{-1}}$
Heat Capacity	C_{thermal}	$1.7677 \cdot 10^{4}$	$\mathrm{J\,K^{-1}}$
Additive Parts	Y_{add}	0.0147	$\mathrm{kg\,kg^{-1}}$
	T_{add}	316.6959	K
	F_{add}	0.1483	$\mathrm{kg\,s^{-1}}$